ELSEVIER

Microelectronics Journal 33 (2002) 161–170

Microelectronics Journal

www.elsevier.com/locate/mejo

Optical MTF and quantum efficiency analysis in a finite slab

D. Abbott*

Centre for Biomedical Engineering (CBME) and Department of Electrical & Electronic Engineering, Adelaide University, Adelaide, SA 5005, Australia

Accepted 21 August 2001

Abstract

The formula for quantum efficiency in a semiconducting material was first derived by Seib in 1974 for a semi-infinite slab of semiconducting material. Seib's first-order analysis considered the effect of absorption coefficient, minority carrier diffusion length and depletion width. However, for modern devices on epitaxial material, smart sensors, quantum well devices, etc., the semi-infinite slab approximation breaks down. Here, we present the derivation for a finite slab that considers the thickness of the layer as a fourth parameter. We present a case study analyzing quantum efficiency, and hence MTF, in epitaxial silicon versus bulk gallium arsenide. © 2002 Published by Elsevier Science Ltd.

Keywords: Internal quantum efficiency; Modulation transfer function; Optical image sensors; Optical smart sensors; Photodetection

1. Introduction

An analysis that compares the optical absorption coefficients of GaAs and silicon, shows that GaAs is optically the superior material for use in photodetection and imaging. The governing equation for the penetration of light into the material is given by Lambert's law of absorption (also known as Bouguer's or Beer's law),

$$\Phi(x) = \Phi_o e^{-\alpha x}$$

where α is called the absorption coefficient. Comparison of the absorption coefficients of GaAs and silicon against wavelength (λ), clearly highlights the superiority of GaAs.

The absorption length or penetration is given by α^{-1}. So for instance, the percentage of light absorbed within two absorption lengths, i.e. $2\alpha^{-1}$, is $100(1 - e^{-2}) = 86\%$. Lambert's law is graphically illustrated in Fig. 1 for GaAs.

To understand what this means, from Table 1 we deduce that at $\lambda = 0.6$ μm, 86% is absorbed within 0.4 μm for GaAs and within 4 μm for Si.

The implication is that GaAs is a more efficient photocollector as most of the light is detected near the surface, where transistor action collects the photocharge. Improved spatial resolution is expected, as a result, and fewer wasted carriers imply improved quantum efficiency and hence greater responsivity.

The absorption length dependence on wavelength, in GaAs, is displayed in Fig. 2. The positions of the cut-off wavelengths in GaAs and Si are indicated showing that GaAs is closer to the peak response of the human eye and is better placed with respect to the visible spectrum. Indeed, at 5.5 μm, the peak eye response, the absorption length for GaAs is precisely in the channel region — whereas for silicon, absorption at this wavelength, occurs well into the substrate where many carriers recombine and are thus not collected.

The relative positions of GaAlAs and red He–Ne lasers are indicated on the curve, showing that GaAlAs emitters are suited for investigations at channel–substrate interface depths, whereas red He–Ne lends itself for observing substrate effects. Fig. 2, clearly shows that neither GaAs nor silicon can intrinsically achieve sensitivity in the standard 3–5 μm MWIR or 8–12 μm LWIR infrared bands.

However, a GaAs imager can be extended to operate in the Near IR waveband, as indicated in Fig. 2. The introduction of states in the forbidden gap, introduced intentionally by impurities such as chromium, provide 'stepping stones' for electrons to traverse the bandgap via excitation from these lower energy wavelengths. This technique is well known in silicon infrared imagers, where the impurity used is typically indium. Such imagers are called *extrinsic* detectors.

As indicated, an alternative scheme to achieve Near IR sensitivity, is to utilize the *internal photoemission* effect. Internal photoemission occurs when the incident light frees electrons from the surface of the gate metal, which

* Tel.: +61-8-8303-5748; fax: +61-8-8303-4360.
E-mail address: dabbott@eleceng.adelaide.edu.au (D. Abbott).

0026-2692/02/$ - see front matter © 2002 Published by Elsevier Science Ltd.
PII: S0026-2692(01)00115-X

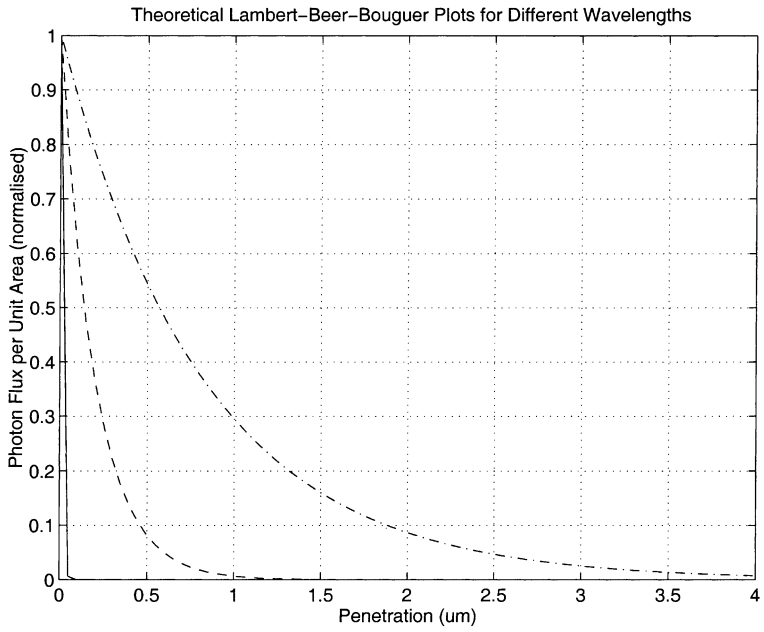

Fig. 1. Lambert's Law of Absorption for GaAs. Solid line: $\lambda = 0.4$ μm. Dashed line: $\lambda = 0.6$ μm. Chained line: $\lambda = 0.8$ μm.

are then collected if they have enough energy to jump the gate Schottky barrier. Now, the Schottky barrier height for a MESFET is about 0.8 eV, whereas the GaAs and Si band-gaps are 1.4 and 1.1 eV, respectively — therefore, less energy is required for an electron to jump the Schottky barrier than to jump a band gap. Thus, internal photoemission provides sensitivity to longer wavelengths of lower energy, namely in the Near IR band. Commercial Si imagers, using internal photoemission, are available on the market — translating this scheme over to GaAs would be an interesting open question.

Fig. 3 highlights the superiority of GaAs over Si, for visible band detection, showing clearly that in GaAs the entire visible spectrum is absorbed close to where transistor action occurs, whereas for silicon the longer visible wavelengths are absorbed well into the substrate. Electrons that are generated by this absorption, in the silicon substrate, either recombine (and are therefore wasted) or diffuse to the channel region causing an unfortunate degradation in spatial resolution.

Note that size and position of the channel/substrate depletion region, in Fig. 3, is for a GaAs MESFET. For a typical silicon MOSFET, the depletion region will be a little smaller, this further highlights the superiority of the GaAs MESFET for photodetection.

Table 1
Absorption coefficients

Absorption coefficients		
λ (μm)	GaAs α^{-1} (μm)	Si α^{-1} (μm)
0.4	0.01	0.1
0.6	0.20	2.0
0.8	0.82	12.0

2. Quantum efficiency formulae

Before we can compare the quantum efficiencies of GaAs and silicon imagers, we must first carefully discuss a few esoteric subtleties.

Firstly, it should be noted that minority carriers in silicon substrates have diffusion lengths much larger than the pixel size. Hence, in order to reduce pixel crosstalk, silicon imagers are all exclusively fabricated on epitaxial substrates. The substrate under the epilayer is heavily doped

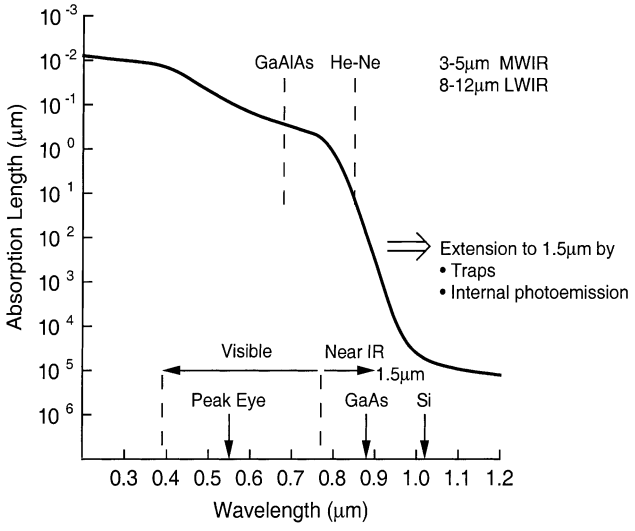

Fig. 2. GaAs absorption length dependence on wavelength.

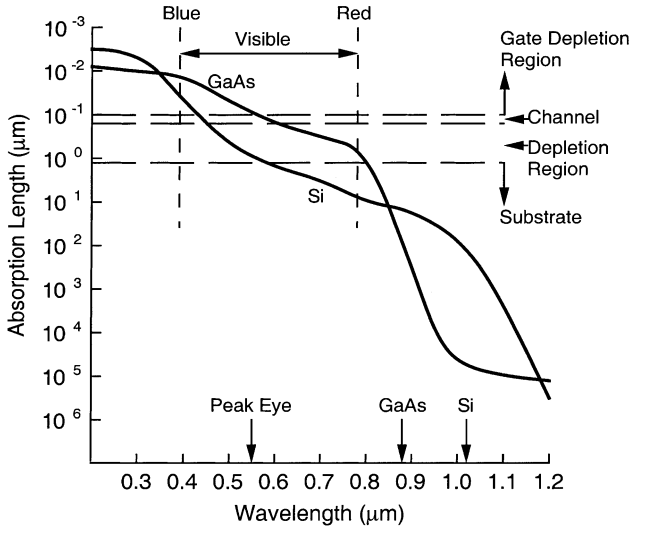

Fig. 3. GaAs versus Si absorption length comparison.

so that stray carriers quickly recombine and do not find their way to neighboring pixels. Unfortunately, the quantum efficiency is thereby reduced, as a large number of carriers are forced to recombine in this way.

Due to the unusual hi–lo junction [1] ($n+$/SI) situation present in a bulk GaAs imager, it is the *majority* carriers that are being collected — hence, a bulk substrate is appropriate for a GaAs imager. Therefore, for our GaAs case, it is appropriate to use the formula for quantum efficiency that approximates the bulk substrate to a semi-infinite slab giving (see Appendix A).

$$\eta_{\text{bulk}} = T(\lambda)\left(1 - \frac{e^{-\alpha W}}{1+\alpha L_o}\right). \tag{1}$$

By contrast, in a typical silicon imager it is the *minority* carriers that are collected and there is a quantum efficiency degradation due to minority carriers recombining before they are collected. As this situation does not occur in our GaAs scenario, we may simulate this by setting the minority carrier diffusion length $L_o = 0$ in Eq. (1).[2]

For the epitaxial silicon case, the semi-infinite slab assumption of Eq. (1) is no longer valid as the epi-layer is thin and of the order of $h = 15$–25 μm. In Appendix B, we show that if we consider a finite slab, the appropriate quantum efficiency formula for epi is

$$\eta_{\text{epi}} = T(\lambda)\left(1 - \frac{e^{-\alpha W}}{1+\alpha L_o} - \frac{\alpha L_o e^{-\alpha W}}{\alpha^2 L_o^2 - 1}\,\frac{e^{-h/L_o} - e^{-h\alpha}}{\sinh(h/L_o)}\right). \tag{2}$$

[1] This assumes devices with no p-buffer layer and that the SI substrate is slightly n-type, and hence, we have a hi–lo junction situation.

[2] This equation should not be confused with the expressions for quantum efficiency which consider collection of holes by the gate, producing a gate photocurrent. We are considering the more general case of electron collection producing channel photocurrent.

If we let

$$\eta_{+} = T(\lambda)\frac{\alpha L_o e^{-\alpha W}}{\alpha^2 L_o^2 - 1}\,\frac{e^{-h/L_o} - e^{-h\alpha}}{\sinh(h/L_o)}$$

we see the remarkable result that $\eta_{\text{epi}} = \eta_{\text{bulk}} - \eta_{+}$, where η_{+} is the is the quantum efficiency of the highly doped substrate beneath the epitaxial layer. Notice this formula assumes that recombination in the highly doped substrate is instantaneous — this approximation is accurate for most practical cases. The ability to separate η_{epi} into two clearly identifiable terms is significant, as the modulation transfer function (MTF) can then also be separated and the two terms can be analyzed separately in a physically meaningful way.

Both Eq. (2) and the realization that it can be separated into two physically identifiable terms has not been reported in the open literature. The quantum efficiency formulae are generally poorly presented and ill conceived in the literature. For instance, a recent attempt at a formula [1] for η_{epi} is clearly dimensionally incorrect, does not have separable terms and under some conditions produces values greater than unity! Note that our expression (Eq. (2)) has all the expected features. Each term is dimensionless, i.e. each argument is a ratio of two lengths or an absorption coefficient times a length. This is an important feature, which is missing, in erroneous attempts found in the literature. Also for $h \to \infty$ our expression reduces to the semi-infinite case. Our function is also well behaved in that quantum efficiency goes down for increasing absorption length, as expected, and goes up for increasing diffusion length. Another important feature is that, by inspection, Eq. (2) always stays below unity.

There is also some confusion in the literature over Eq. (1). Our equation agrees with the derivation in the seminal work of Seib [2] and with a fair body of literature. However, there is an erroneous formula due to Barbe [3] that appears to have insidiously propagated, unchallenged, into some of the literature, such as in McCaughan [4]. Barbe's expression is in terms of MTF and therefore we plot the MTF expressions for both Barbe and Seib in Fig. 4, showing that Barbe's expression is clearly too optimistic.

3. Quantum efficiency and responsivity

Using Eqs. (1) and (2), we can now analyze the quantum efficiency and hence the responsivity in both the silicon and GaAs devices — these formulae were used to plot Fig. 8.

At the red end of the spectrum, i.e. 8 μm, we find that the GaAs device has about twice the quantum efficiency of a comparable silicon device. Some of this advantage will be lost due to the opaque gates in GaAs.

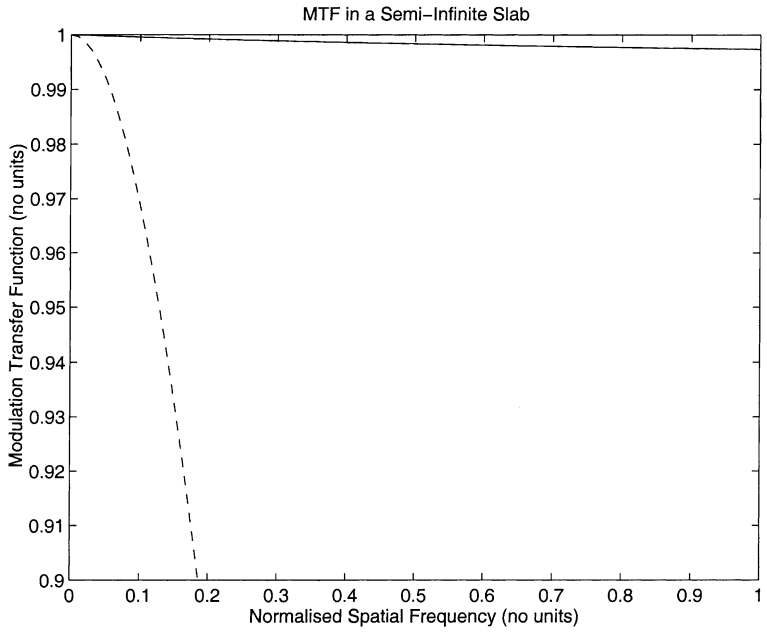

Fig. 4. MTF due to diffusion. A comparison of the traditional formula due to Seib (dashed line) and the formula due to Barbe (solid line).

Responsivity is related to the quantum efficiency by,

$$R_\lambda = \frac{q\lambda}{hc}\eta \text{ A/W}$$

For all wavelengths, the total is

$$R = \frac{\int_0^\infty R_\lambda W_\lambda \, d\lambda}{\int_0^\infty W_\lambda \, d\lambda}$$

where, by Planck, radiated power,

$$W_\lambda = \frac{2\pi c^2 h}{\lambda^5 (e^{hc/\lambda kt} - 1)} \text{ W/m}^3$$

where this curve is illustrated in Fig. 5.

For reference, a silicon MOS CCD, has typically, $R \approx 50$ mA/W (3000 K tungsten source). We expect to exceed this with a GaAs imager and values are predicted as follows.

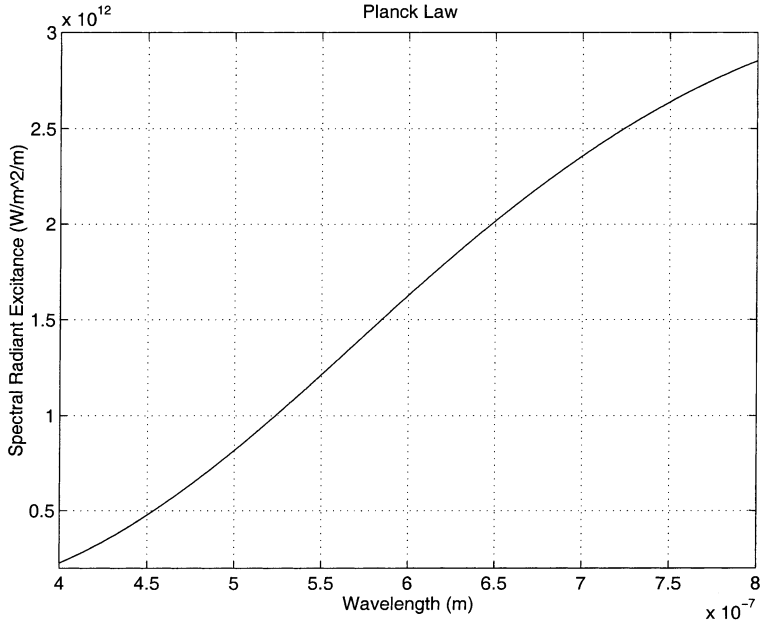

Fig. 5. Planck's law curve, W_λ. Area under curve for visible wavelength range is 5.31×10^5 W/m^2. Total area under the curve for all wavelengths, given by Stefan's Law, is 46×10^5 W/m^2.

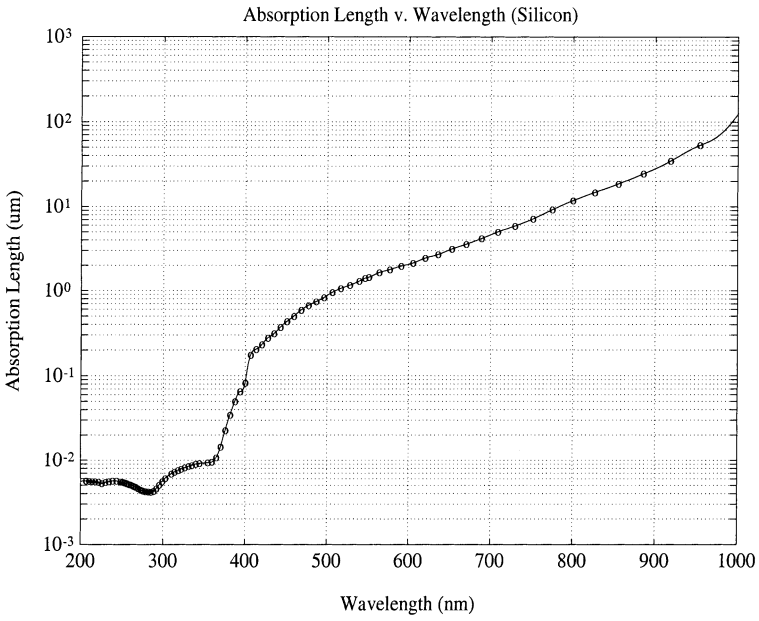

Fig. 6. Measured absorption length against wavelength for silicon.

Figs. 6 and 7 show measured absorption lengths for silicon and gallium arsenide. From these curves the predicted quantum efficiencies are plotted in Fig. 8.

The superior quantum efficiency of GaAs over silicon, as seen in Fig. 8, is due to the shallower absorption lengths and majority carrier collection process in the GaAs imager. In silicon imagers, minority carriers are collected and so there is a degradation in quantum efficiency due to recombination processes. For the purpose of comparison, we have assumed a transmission coefficient of unity, this simplification does not make a difference to our conclusions. In Fig. 8, a depletion region width of $W = 0.1$ μm corresponds to that under the gate. The improved quantum efficiency curves with $W = 1$–2 μm, simulate the expected effect of the substrate/channel depletion region working together with the gate depletion region. As the imager is a low-frequency device, we expect the substrate/channel depletion region to take part in the collection process, leading to excellent quantum efficiency.

From the quantum efficiency curves we can now apply

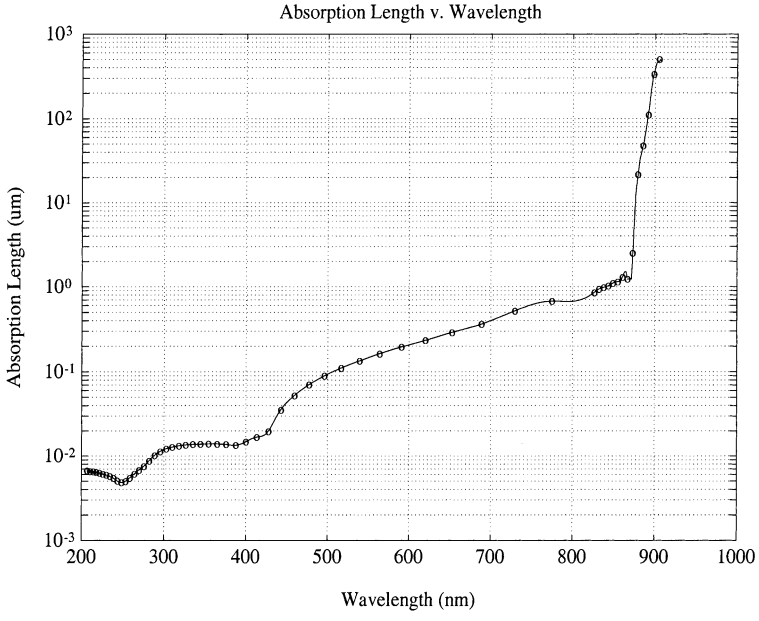

Fig. 7. Measured absorption length against wavelength for GaAs.

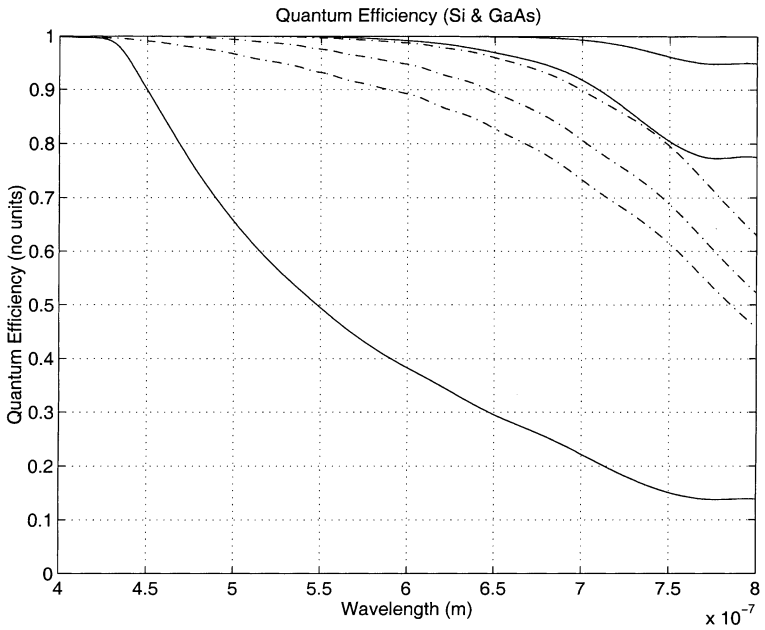

Fig. 8. IQE versus wavelength. Dashed lines, silicon $W = 5$, 2 and 0.5 μm. Solid lines GaAs $W = 2$, 1 or 0.1 μm. Quantum efficiency increases with depletion width W. Transmission coefficient is set at unity.

Planck's law to calculate the responsivities. Figs. 9 and 10 show the weighted responsivities for silcon and gallium arsenide.

Total responsivity, over the visible spectrum, is determined by evaluating the areas under the curves in Figs. 9 and 10 and then dividing by the total area under the Planck's Law curve $= 46 \times 10^5$ W/m^2 (see Fig. 5).

A typical tungsten light source can be simulated by inserting a temperature of 3000 K into the Planck equations and the resulting responsivities are displayed in Table 2.

The results for silicon, are a little larger compared to, say, 50 mA/W for a typical silicon XY array imager with $W =$ 5 μm. This is because we have omitted the effect of the transmission coefficient and furthermore we have assumed a fixed depletion width. In reality the depletion width diminishes as photocharge collects — however the comparison between GaAs and silicon is still valid if we make the simplification of a fixed depletion width. Table 2 shows that for GaAs operating with just the gate depletion region, $W = 0.1$ μm, the responsivity is inferior. However, if we

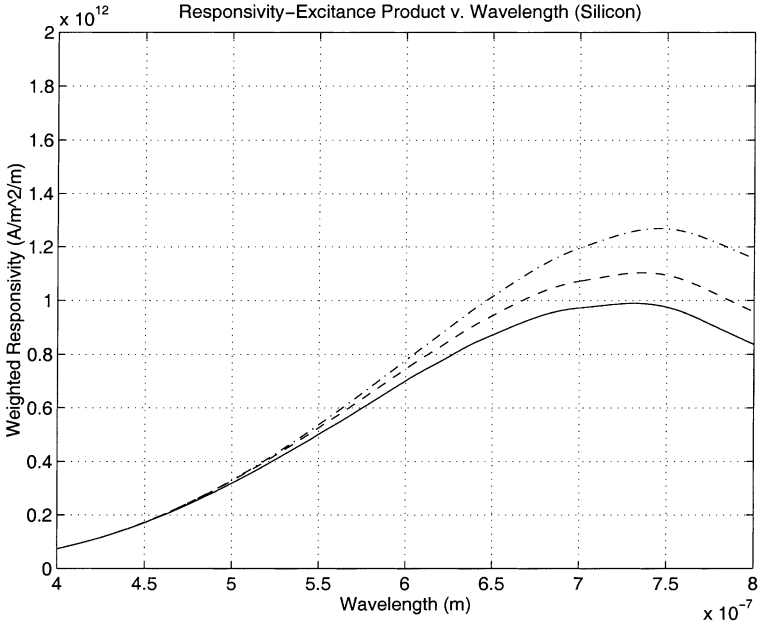

Fig. 9. Weighted reponsivity versus wavelength for silicon. Solid line: $W = 0.5$ μm. Dashed line: $W = 2$ μm. Chained line: $W = 5$ μm.

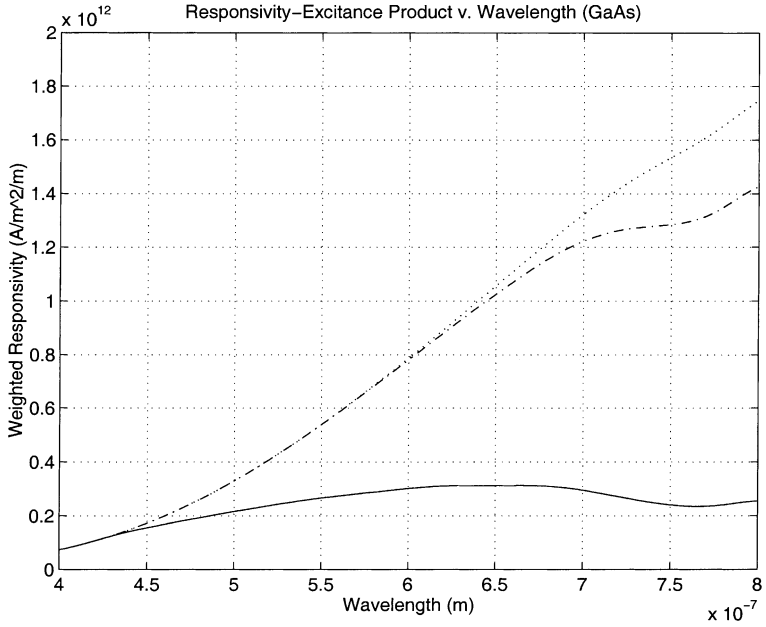

Fig. 10. Weighted responsivity versus wavelength for GaAs. Solid line: $W = 0.1$ μm. Chained line: $W = 1$ μm. Dotted line: $W = 2$ μm.

include the channel/substrate region, with $W = 0.2$ μm, the responsivity in GaAs is about 20% larger than in silicon. Furthermore, if we take into account that the channel/substrate region has a fixed potential across it, in contrast to the silicon *XY* array where the depletion region shrinks during photocollection, we can expect that GaAs would have up to a factor of five improvement in responsivity. This means that a 'fingered gate' pixel design, may still equal or even out-perform silicon, despite the presence of opaque gates.

4. MTF analysis — spatial degradation by diffusion

According to the Lambertian exponential law for the absorption of light, we see that 63% is absorbed within one absorption length. We have seen that the absorption lengths, for visible light in GaAs, are all of comparable order to the vertical transistor dimensions. The implication of photocharge being collected at these shallow depths is that the GaAs MESFET is an efficient photocollector. Furthermore, if most of the carriers are efficiently collected then the number of stray carriers spreading, thereby causing spatial degradation of the image, is low. Hence, we expect the spatial resolution of a GaAs imager to be excellent. The channel/substrate depletion region is expected to assist in this regard, by deflecting minority carriers into the substrate and sweeping stray electrons into the collecting channel.

Table 2
GaAs versus Si Responsivity

Type	Depletion W (μm)	Area under curve (W/m^2)	Responsivity (mA/W)
Si	0.5	2.37×10^5	51
Si	2.0	2.95×10^5	56
Si	5.0	2.81×10^5	61
GaAs	0.1	1.00×10^5	22
GaAs	1.0	2.95×10^5	64
GaAs	2.0	3.25×10^5	71

The quantitative comparison of GaAs and silicon, at first sight, appears to be difficult due to the fact that our GaAs example is on a bulk substrate, whereas silicon imagers are on epitaxial substrates. Hence, we are not comparing like with like. A thin epilayer gives rise to a poor quantum efficiency but an excellent spatial resolution, whereas a bulk substrate gives an improved quantum efficiency at the expense of spatial resolution. So how can we make a fair comparison that takes into account this trade-off? The answer is to compare GaAs with silicon, not in terms quantum efficiency or raw spatial resolution *per se*, but in terms of a special figure of merit known as the MTF. An ideal MTF has the value of unity and it has the behavior that if either quantum efficiency or spatial resolution decreases, then MTF also decreases below unity. The definition of MTF is simply [2]

$$\mathrm{MTF} = \frac{\eta_k}{\eta}$$

where η_k is given by the same formula as the quantum efficiency, η, but with each L_o term substituted by $\sqrt{1/L_o^2 + (2\pi k)^2}$ and k is the spatial frequency.

This is plotted in Fig. 11, where the importance of epi rather than bulk substrates for silicon is demonstrated. Although the diffusion curve for a wavelength of 550 nm in bulk is acceptable, the MTF for 800 nm is severely degraded in bulk compared to epi. The geometrical-only

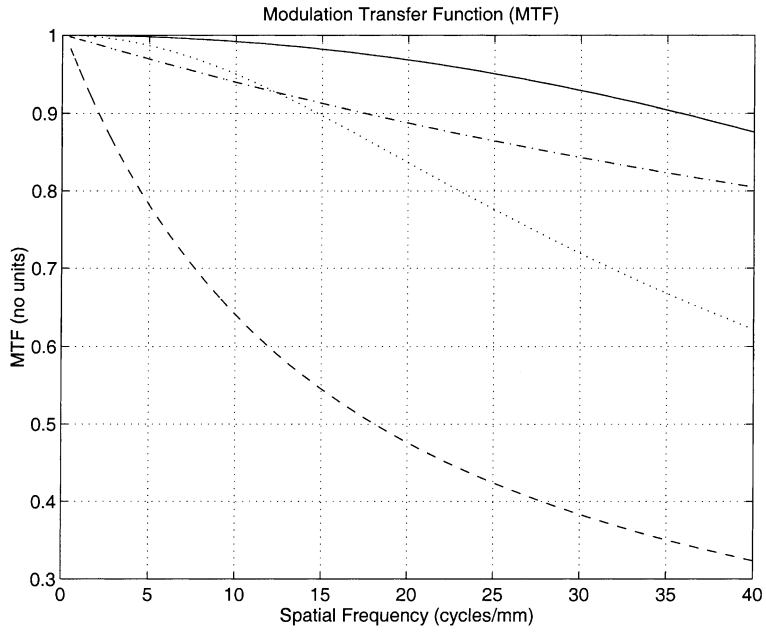

Fig. 11. Theoretical MTF versus spatial frequency. Diffusion-only curves are: Si bulk, 550 nm (chained line) Si epi, 800 nm (dotted line); Si bulk, 800 nm (dashed line). Geometrical-only curve is for a 7/20 aperture to pitch ratio and the GaAs case matches this curve (solid line).

curve is obtained from the usual sinc function expression and represents the ideal case in absence of diffusion effects. Due to the hi–lo n^+/SI junction majority carriers are collected; hence, the diffusion term vanishes and our GaAs case corresponds to the ideal geometrical curve. This result is attractive for HDTV detector array applications, where high pixel densities are more susceptible to crosstalk by diffusion.

5. Conclusions

In the first order analysis of quantum efficiency, we have disputed the equation for quantum efficiency in a frontside illuminated finite slab given in recent literature. From first principles, we derive the correct first order equation, which has not been previously reported in the open literature. This result is significant as the equation can be separated into two physically meaningful terms. This new perspective will be useful for simplifying MTF analysis in epi substrates. Furthermore, we have disputed the MTF equation in bulk due to Barbe and have confirmed, from first principles, the validity of Seib's bulk equation. An open question is to extend our analysis to include the effect of surface states and other second order effects.

We have shown that due to the superior absorption coefficients in GaAs, improved quantum efficiency is expected. Furthermore for a hi–lo n/SI junction in GaAs, majority carriers are collected and this leads to improved spatial resolution. This advantage is presented in the form of MTF plots, showing superior overall MTF of GaAs over silicon. Future work could try to exploit this improved spatial resolution for, say, HDTV sensors.

Acknowledgements

This work was supported by the Australian Research Council and the Sir Ross and Sir Keith Smith Fund (Australia).

Appendix A. Quantum efficiency in a semi-infinite slab

Consider a semi-infinite slab of semiconductor material. Let the surface be at $x = 0$ and the backside be at $x = \infty$. The continuity equation balance for generation and recombination under steady-state is

$$-D\nabla^2 n + \frac{n}{\tau} = G \tag{A1}$$

where D is the diffusion constant, n is the minority carrier concentration in the undepleted region, τ is minority carrier lifetime and G the electron–hole pair generation rate. We shall use n to denote either n or p type carriers as this analysis is independent of whether electrons or holes are the minority carriers, so long as the correct coefficient values for holes or electrons are used in any particular instance. The generation rate G is given by

$$G = \Phi\alpha e^{-\alpha x} \tag{A2}$$

where Φ is the incident photon flux per unit area and α is the absorption coefficient. Combining the above equations with the expression for minority carrier diffusion length,

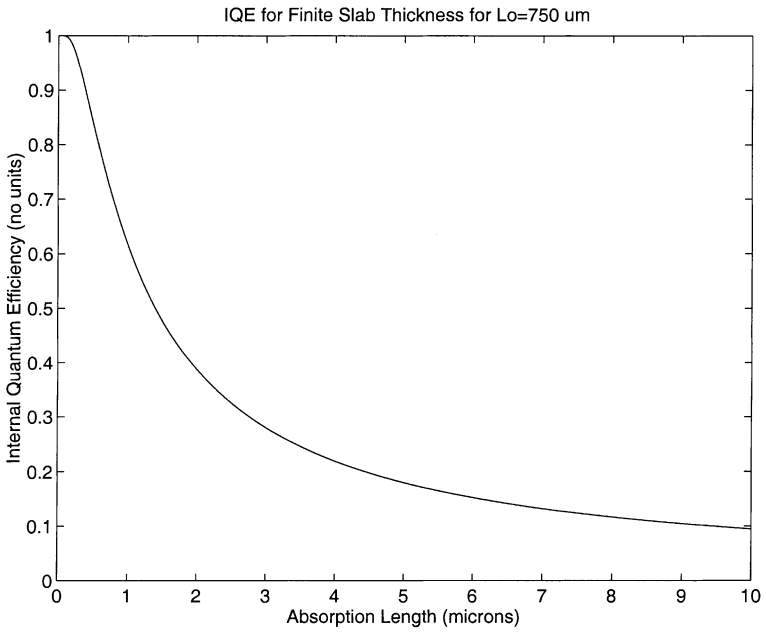

Fig. 12. IQE versus absorption length.

$L_o = \sqrt{D_\tau}$, we get

$$\frac{d^2n}{dx^2} - \frac{n}{L_o^2} = \frac{-1}{D}\Phi\alpha e^{-\alpha x} \tag{A3}$$

Using the solution of the form,

$$n = Ae^{-\alpha x} + Be^{-x/L_o} + Ce^{x/L_o} \tag{A4}$$

we assert boundary conditions at the depletion edge $x = W$, $n = 0$ and at the slab backside $x = \infty$, $n = 0$, yielding

$$A = \frac{\alpha L_o^2 \Phi}{(1-\alpha^2 L_o^2)D}, \qquad B = -Ae^{(1/L_o-\alpha)W}, \qquad C = 0$$

The steady state carrier flux is given by

$$J = \int_0^W G\,dx + D\frac{\partial n}{\partial x}|_{x=W} \tag{A5}$$

which becomes

$$J = \Phi(1-e^{\alpha W}) - DA\alpha e^{-\alpha W} - \frac{DB}{L_o}e^{-W/L_o}$$

and by substituting in the expressions for A and B,

$$J = \Phi(1-e^{\alpha W}) + \frac{\alpha L_o \Phi e^{\alpha W}}{1+\alpha L_o}$$

hence, internal quantum efficiency (IQE) which is given by, $\eta = J/\Phi$, becomes

$$\eta = 1 - \frac{e^{-\alpha W}}{1+\alpha L_o} \tag{A6}$$

Appendix B. Quantum efficiency in a finite slab

Consider a slab of semiconductor material, with finite thickness, h. For mathematical convenience, let the surface be at $x = -W$, the depletion region edge be at $x = 0$ and the backside be at $x = h - W$. We can rewrite the continuity equation, in the last section, as

$$\frac{d^2n}{dx^2} - \frac{n}{L_o^2} = \frac{-1}{D}\Phi\alpha e^{-\alpha(x+W)} \tag{B1}$$

Again, using the solution of the form,

$$n = Ae^{-\alpha x} + Be^{-x/L_o} + Ce^{x/L_o} \tag{B2}$$

we assert boundary conditions at the depletion edge $x = 0$, $n = 0$ and at the slab backside $x = h - W$, $n = 0$, yielding

$$A = \frac{\alpha L_o^2 \Phi}{(1-\alpha^2 L_o^2)D}, \qquad B = -A\frac{1-e^{-(h-W)(\alpha+1/L_o)}}{1-e^{-2(h-W)/L_o}},$$

$$C = -A\frac{1-e^{-(h-W)(\alpha-1/L_o)}}{1-e^{-2(h-W)/L_o}}$$

The steady state carrier flux is given by

$$J = \int_{-W}^0 \Phi(1-e^{-\alpha W}) + D\frac{\partial n}{\partial x}|_{x=0} \tag{B3}$$

which becomes

$$J = \Phi(1-e^{\alpha W}) - DA\alpha - \frac{DB}{L_o} + \frac{DC}{L_o}$$

and by substituting in the expressions for A, B and C, after

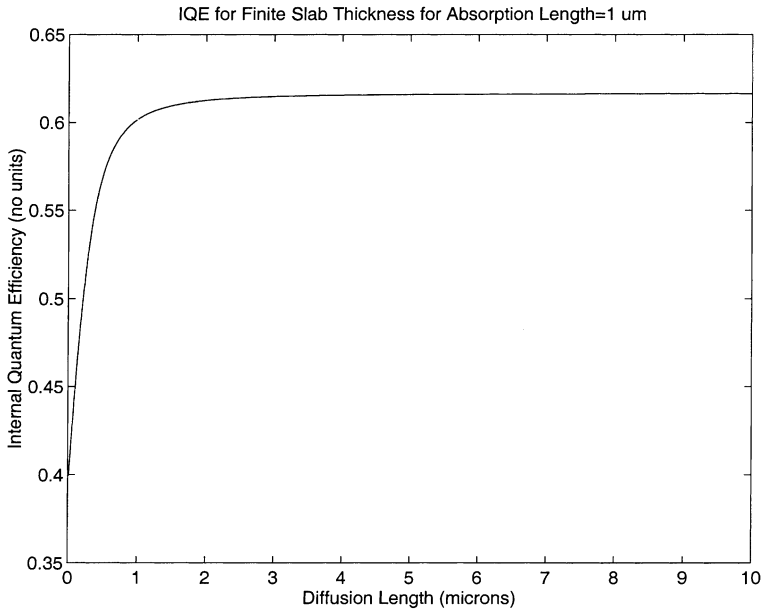

Fig. 13. IQE versus absorption length.

some manipulation, using $\eta = J/\Phi$, we get

$$\eta = 1 - \frac{e^{-\alpha W}}{1 + \alpha L_o} - \frac{\alpha L_o e^{-\alpha W}}{\alpha^2 L_o^2 - 1} \frac{e^{-h/L_o} - e^{-h\alpha}}{\sinh(h/L_o)} \quad \text{(B4)}$$

This equation shows that the quantum efficiency equals that of the semi-infinite case *plus* a (negative) second order term. It is quite remarkable and elegant that these two terms can be separately identified. Both this expression and the realization that the semi-infinite case *plus* a second order term yields the finite slab case, seem to appear nowhere in the literature. Note that this expression has all the expected features. Each term is dimensionless, i.e. each argument is a ratio of two lengths or an absorption coefficient times a length. This is an important feature that is missing in some erroneous attempts found in the literature. Also for $h \to \infty$ the expression reduces to the semi-infinite case.

The function is also well behaved in that IQE goes down, as expected, for increasing absorption length, Fig. 12, and goes up for increasing diffusion length, Fig. 13. Another important feature is that, by inspection, IQE always stays below unity — this is illustrated for specific examples in the graphs.

References

[1] A.J.P. Theuwissen, Solid-State Imaging with Charge-Coupled Devices, Kluwer, Dordrecht, 1995, p. 135.
[2] D.H. Seib, Carrier diffusion degradation of modulation transfer function in charge coupled imagers, IEEE Trans. E. D. 21 (3) (1974) 210–217.
[3] D.F. Barbe, Imaging devices using the charge-coupled concept, Proc. IEEE 63 (1975) 38–67.
[4] D.V. McCaughan, B.R. Holeman, in: M.J. Howes, D.V. Morgan (Eds.), Charge-Coupled Devices and Systems, Wiley, New York, 1979, pp. 241–295, chapter 5.